Investigations and Design Considerations for High-Speed Wireless Charging Module Incorporating Supercapacitors in the Superconducting Hyperloop Train

Yoon Do CHUNG*, and ChangYoung LEE**
*Department of Electrical Engineering, Suwon Science College, Hwaseong-si, Gyeonggi-do, 18516, Korea
**Team of High Speed Train, Korea Railroad Research Institute, Uiwang-si, Gyeonggi-do, 16105, Korea

Abstract
Magnetic resonant coupling-based wireless power transfer (MRC-WPT) has gained considerable attention as a viable approach for high-power energy delivery, offering enhanced safety and operational flexibility—particularly within industrial automation and advanced transportation infrastructures. This technology is especially relevant for applications such as autonomous electric vehicles, electric trams, and next-generation high-speed transit systems like Hyperloop. Traditional energy transmission techniques, including wired interfaces through pantograph mechanisms, tend to escalate infrastructural expenses—most notably in enclosed environments such as tunnels—and may adversely affect the dynamic performance of systems employing magnetic levitation, including MAGLEV and superconducting propulsion platforms. Despite its advantages, WPT systems designed to supply power to high-temperature superconducting (HTS) levitation modules face fundamental challenges, primarily due to the significant inductive time constants associated with superconducting coils, which hinder efficient energy storage and rapid power transfer. In addition, the deployment of such systems incurs high capital and operational expenditures due to the reliance on complex auxiliary subsystems, including high-frequency power amplifiers and high-current rectification modules. Recently, supercapacitor technologies have emerged as promising candidates for energy buffering applications across various domains—including portable industrial equipment, detachable battery systems, and embedded sensors—owing to their high-power discharge capability and suitability for low-voltage operation. In this context, the present study investigates the potential of a fast-charging wireless power charging system (FC-PCS) that integrates super-capacitive energy storage. The research includes experimental assessments utilizing a 58 Farad supercapacitor module energized by a 200-watt, 370-kHz RF power source under variable magnetic loading conditions.

Keywords : Fast wireless power supply, hyperloop, supercapacitor, superconducting levitation magnet.

1. Introduction

The Hyperloop represents a next-generation, ultra-high-speed (up to 1200 km/h) ground transportation system designed for both passenger and freight applications. Operating within a low-pressure environment, the system benefits from minimal aerodynamic drag, resulting in enhanced energy efficiency. Owing to its reliance on contactless levitation and propulsion mechanisms housed within a vacuum tube, electrical power for these systems must be delivered from outside the vacuum environment. Recent advancements in high-speed transportation emphasize the use of superconducting levitation magnets, which provide strong levitation forces that not only improve system stability but also contribute to reduced infrastructure costs. Consequently, the design and optimization of high-temperature superconducting (HTS) magnets have become a key area of research in transportation engineering [1]–[3]. Despite their economic advantages over low-temperature superconducting (LTS) systems in terms of cooling requirements and overall equipment cost, HTS magnets suffer from current decay during persistent mode operation. Therefore, supplementary power sources are essential to compensate for this decay and maintain consistent levitation performance [4], [5]. Traditional power delivery methods, such as pantograph-based overhead lines, are not well-suited for low-pressure, high-

speed systems like MAGLEV and Hyperloop. These methods not only escalate construction costs but also compromise system stability. As an alternative, Magnetic Resonant Coupling Wireless Power Transfer (MRC-WPT) technology has been proposed as a viable solution [6]–[9], as illustrated in Fig. 1 (a). Wireless power transfer (WPT) enables efficient energy transmission between a source and a load without physical connectors. Due to its advantages including operational convenience, elimination of physical wear, and functionality in constrained environments, the WPT has gained significant attention in various sectors, including medical devices, robotics, and consumer electronics [10]. Fig. 1 (b) presents a conceptual schematic of the proposed FC-PCS module as applied to a superconducting Hyperloop train equipped with a HTS levitation magnet employing Electrodynamic Suspension (EDS) technology.

In recent years, supercapacitors have emerged as efficient energy storage devices across diverse applications, including portable industrial tools, modular electronic devices, and sensor-actuator systems. In biomedical engineering, particularly in magnetic resonance imaging systems, supercapacitors are favored for their ability to provide high power output at low voltage levels [11]–[13]. In light of these considerations, this study proposes a fast-charging power charging system (FC-PCS) integrating a supercapacitor module as a cost-effective and high-energy-density alternative for charging HTS magnets. While supercapacitors offer rapid discharge capabilities, this very feature necessitates precise current regulation to avoid quenching—a phenomenon that can critically impair superconducting systems. In this work, the authors examine the discharge characteristics of a supercapacitor under varying magnet inductances to determine the influence of load impedance on the discharge rate. Specifically, the experimental setup employs a 58 F supercapacitor module charged via a 200 W, 370 kHz RF power supply under different inductive load conditions to evaluate the fundamental performance of the proposed FC-PCS system.

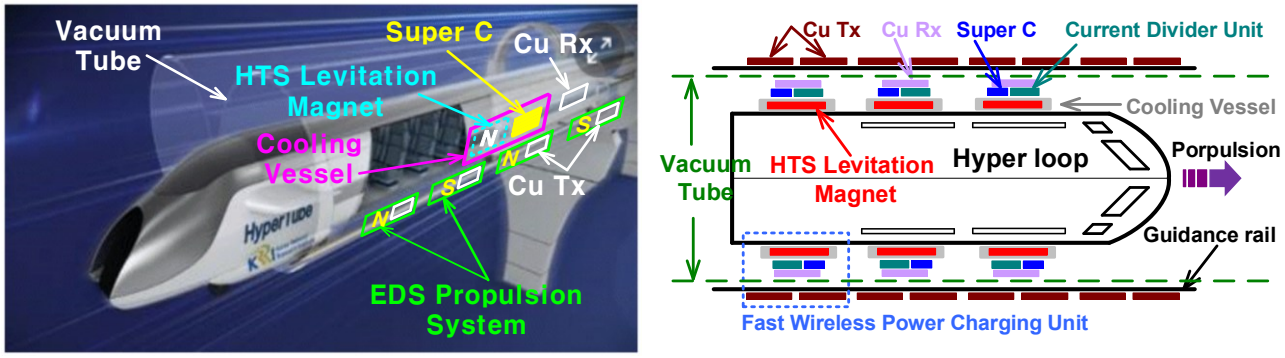

(a) (b)

Fig. 1 Conceptual Illustration of the wireless power charging system incorporating a supercapacitor unit, coupled with electrodynamic suspension (EDS)-based propulsion in the superconducting Hyperloop train (a). Illustration of FC-PCS system via MRCWPT and EDS propulsion-based in the superconducting Hyperloop train (b).

2. Structure and Properties

2.1 Structure of fast wireless power charging unit including supercapacitor for superconducting Hyperloop train

The FC-PCS is structured into three primary functional units: (1) the RF input and transmitting (Tx) coil assembly, (2) the receiving (Rx) coil with rectification stage, and (3) the energy storage section based on a supercapacitor module. The transmitting side includes a 370 kHz RF power generator, an LC-based impedance matching circuit, and a copper Tx resonance coil. The receiving end comprises an Rx coil, which inductively receives the RF signal, and a rectifier bridge circuit that converts the received AC power into direct current. This DC output is used to charge the supercapacitor module, which serves a dual role: functioning as a buffer for the RF generator and as an energy storage unit for applications such as grid stabilization and transient protection.

Both the supercapacitor and the HTS magnet are housed within a shared cryogenic vessel. Given that commercially available supercapacitors are typically rated for minimum operating temperatures down to -40°C, they are thermally isolated from the magnet by a vacuum-insulated chamber to ensure safe operation within the cryogenic environment. The

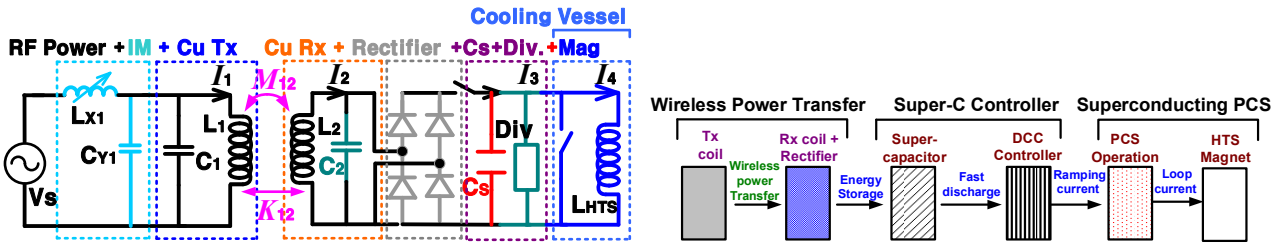

(a) (b)

Fig. 2 (a). Equivalent circuit diagram (a) and schematic diagram for current charging sequences in the FC-PCS module (b).

rectified DC power though relatively small in magnitude is sufficient to gradually charge the supercapacitor due to its ability to deliver high power density with stable output characteristics. This allows even a modest WPT unit to fully charge the storage system. In the configuration tested, the supercapacitor module achieves full charge at 15 V and 3 A within approximately 10 minutes.

Fig. 2 (a) illustrates the equivalent circuit model of the FC-PCS, highlighting the impedance-matched resonant coupling between the Tx and Rx coils. Here, L_1, and L_2 denote the self-inductances of the respective Tx and Rx coils, while capacitors C_1, and C_2, are employed to enhance resonance coupling efficiency. The symbols C_S and L_{HTS} represent the supercapacitor and the HTS levitation magnet, respectively. Fig. 2 (b) provides a system-level schematic of the complete FC-PCS architecture, which consists of six major components:

1. Resonant transmitting coil (Tx)
2. Receiving coil (Rx) with rectification circuit
3. Supercapacitor energy storage unit
4. Discharge current control (DCC) module
5. Persistent current switch (PCS) for superconducting circuits
6. HTS levitation magnet

Notably, the supercapacitor is capable of discharging at currents exceeding 200 A in less than 2 seconds. To prevent thermal or magnetic instability such as a quench event in the superconducting magnet a DCC is incorporated to regulate the discharge rate. This controller enables gradual energy delivery to the magnet, ensuring operational stability and protecting the superconducting state of the system.

2.2 Properties of ultra-supercapacitor

Fig. 3 (a) presents a conceptual schematic of the proposed FC-PCS module as applied to a superconducting Hyperloop train equipped with a HTS levitation magnet employing Electrodynamic Suspension (EDS) technology. The conventional approaches require high-power RF sources and sophisticated rectification units capable of handling large current densities, leading to increased system complexity and cost. Additionally, the large inductance associated with HTS magnets imposes limitations on energy accumulation rates due to their substantial inductive time constants.

Supercapacitors are energy storage devices that combine rapid charging capability with a wide operating temperature range, environmental sustainability, high reliability, and minimal maintenance requirements. These advantages make them well- suited for applications requiring high power density and extended operational lifespans. Structurally, a

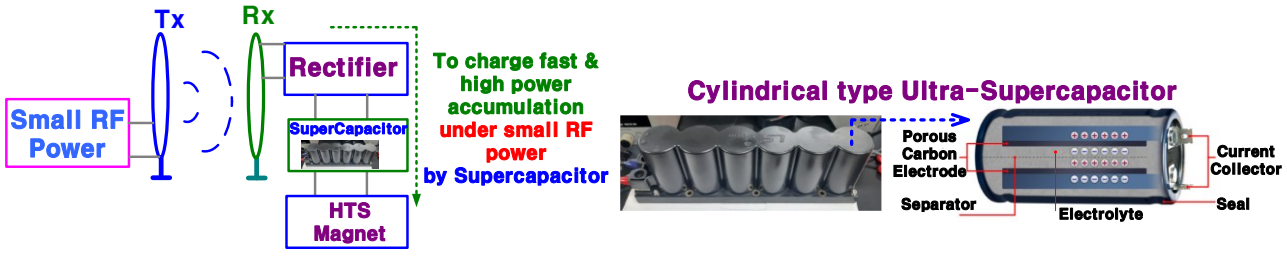

(a) (b)

Fig. 3 Photograph and illustrations of the LS supercapacitor used in testing: structural configuration, and potential variation before and after charging (a). Concept of supercapacitor necessity for HTS magnet to promote the charging speed for magnet under small RF power (b).

within a thermal operating window of approximately –40°C to 200°C. This range enables their integration into diverse environments, including both industrial and vehicular systems.

In terms of performance, supercapacitors offer a high-power density exceeding 1,000 W/kg and a moderate energy density ranging from 5 to 10 Wh/kg. Unlike conventional primary or secondary electrochemical cells (i.e., batteries), supercapacitors store electric energy through the formation of an electric double-layer at the interface between a solid electrode and a liquid electrolyte. This non-faradaic charge storage mechanism contributes to a significantly extended cycle life, typically exceeding one million charge-discharge cycles, making them particularly advantageous in high-cycle applications as shown in Fig. 3 (b).

From a structural classification standpoint, supercapacitors are generally fabricated in either a parallel-plate or a cylindrical configuration. The capacitance of a parallel-plate supercapacitor is determined solely by the physical dimensions specifically, the surface area of the plates and the separation distance between them independent of the amount of stored charge or the applied voltage. In contrast, the capacitance of a cylindrical supercapacitor is governed by geometrical parameters such as the length of the cylinder and the radii of the inner and outer coaxial conductors [14].

Table 1 Dimensional specifications of supercapacitor.

Parameters	Dimension
capacitance	58[F]
max current	210[A]
power	2,100[W/kg]
energy density	3.2[Wh/kg]
rated voltage	16.8[V]
max series voltage	750[V]
operating temperature ranges	-40~65[^{0}C]
isolation DC voltage	5.6[kV]
short circuit current	760[A]
charging/discharging efficiency	95[%]
cycle life	>500,000

Table 2 Dimensional specifications of wireless charging unit and loads.

Parameters	Dimension
length of Tx, Rx copper coils	4.1 / 3.8[m]
coil diameter of Tx and Rx	10[mm]
Q value, impedance, inductance of Tx @ 370kHz	120/25.4[Ω]/11.04[μH]
Q value, impedance, inductance of Rx @ 370kHz	110/24.3[Ω]/ 11.6[μH]
rated power of a bulb as a load	30[W]
rating and resolution of RF power @ 370kHz	1[kW] / 1[W]
Self-inductance of Load A, B @ 60Hz	147 / 205[μH],
total inductance of two inductors connected in series @ 60Hz	307[μH]

3. Experimental Setup and Results

3.1 Experimental setup

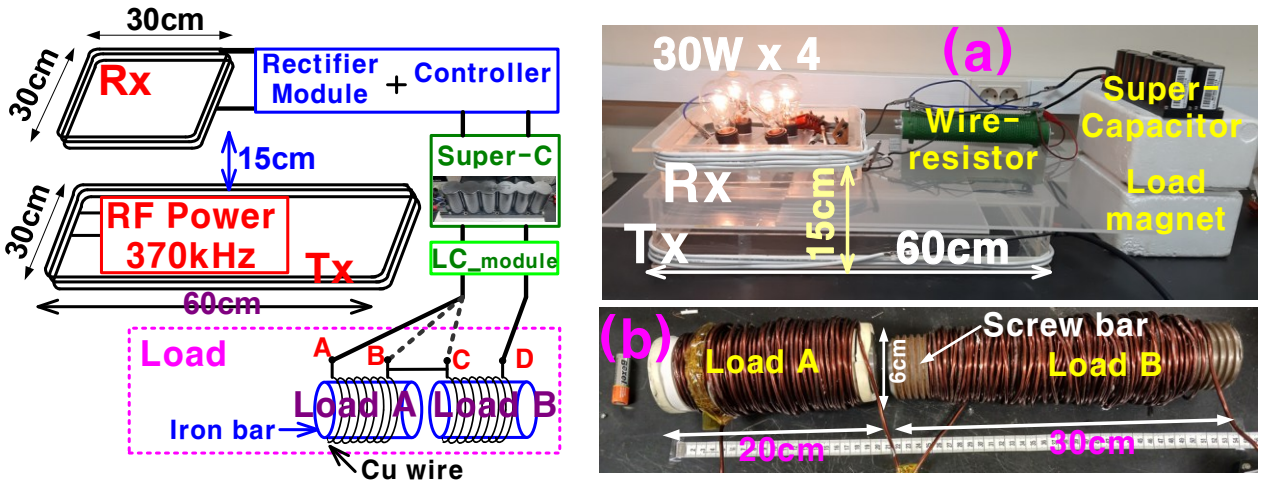

(a) (b)

Fig. 4 Schematic diagram of the assembled test system (a). Photograph of the installed FWPCS including the variable loads (b)

In this experimental study, a cylindrical-type ultracapacitor manufactured by LS was selected as the supercapacitor unit. The detailed specifications of supercapacitor, the wireless charging module and load magnet are summarized in Tables 1 and 2. Fig. 4 presents the experimental setup designed to evaluate the wireless charging performance of the supercapacitor. A 200 W RF generator operating at a frequency of 370 kHz was employed as the primary power source. For the wireless power transmission system, rectangular-shaped helical Tx and Rx coils were utilized. This coil geometry was chosen due to its superior electromagnetic field distribution characteristics when compared with circular or elliptical configurations, thus improving power transfer efficiency. To verify the stability and reliability of the power delivery, four 30 W bulbs were connected to the Rx coil output as resistive loads. In the supercapacitor charging phase, the Rx coil was linked to both a full-wave rectifier bridge and the load magnet as shown in Fig. 4 (a). The impedance matching circuit was carefully designed and fabricated to ensure strong resonant coupling, resulting in a reflected power ratio of less than 5%. This low reflection minimizes thermal losses in the Tx coil even under continuous operation at 200 W input power. The measurements confirm that thermal variation in the supercapacitor is negligible under nominal operating conditions. However, in scenarios where voltage imbalance occurs particularly when the applied voltage exceeds the rated limit an increase in temperature was observed, which could potentially degrade the lifespan and reliability of the supercapacitor.

3.2 Experimental Results

Fig. 5 presents the measured waveforms of voltage and current at both the Tx and Rx coils, along with the rectified voltage signal observed at the supercapacitor under no-load conditions. The WPT system demonstrated a transfer efficiency exceeding 65% at a coil separation distance of 10 cm. Considering the rated voltage limit of the supercapacitor (16.8 V), the system was configured to supply a regulated voltage below 15 V, accompanied by a charging current of approximately 0.77 A, as depicted in Fig. 5 (b). Although the supercapacitor operates at relatively low voltage levels, it supports a high permissible current. This characteristic necessitates the integration of a power control mechanism within the wireless charging system to ensure safe energy transfer. Notably, in typical WPT systems, voltage waveforms are more effectively transmitted across the inductive link than current waveforms. Accordingly, a power-divider controller is placed between the rectifier and the supercapacitor to regulate the delivered power, maintaining it within the safe operating limits of the storage unit.

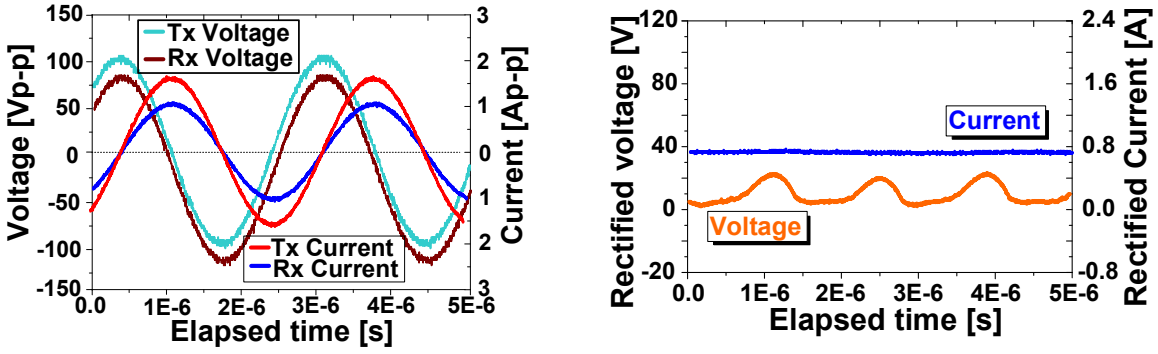

(a) (b)

Fig. 5 Experimental waveforms of voltage and current at the Tx and Rx coils under 200 W RF generator excitation (a), and the rectified voltage and current waveforms across the supercapacitor under no-load condition (b).

Fig. 6 illustrates the time-dependent charging behavior of the supercapacitor under no-load conditions over a 10-minute period. The supercapacitor reaches full charge in approximately 9 minutes and 25 seconds, attaining a peak voltage close to 20 V. Upon reaching this fully charged state, the voltage stabilizes below the maximum rated value, while the charging current approaches zero, indicating equilibrium. These results suggest that if the system is capable of supplying a higher current within the allowable voltage range, the overall charging time could be further reduced.

Fig. 7 displays experimental measurements of the charging voltage and current profiles when the supercapacitor is connected to various inductive loads. The inductances of the tested magnets were 147 μH, 205 μH and 307 μH, respectively. Although the supercapacitor is capable of delivering peak currents up to 200 A, the measurement system was limited to observing ramping currents up to approximately 30 A. Figs. 7 (a) through 7 (c) show the time-domain charging profiles over a 120 ms and 240 ms interval for the inductive loads. The measured ramping current durations corresponding to the inductance values of 147 μH, 205 μH, and 307 μH were 12 ms, 15 ms, and 85 ms, respectively.

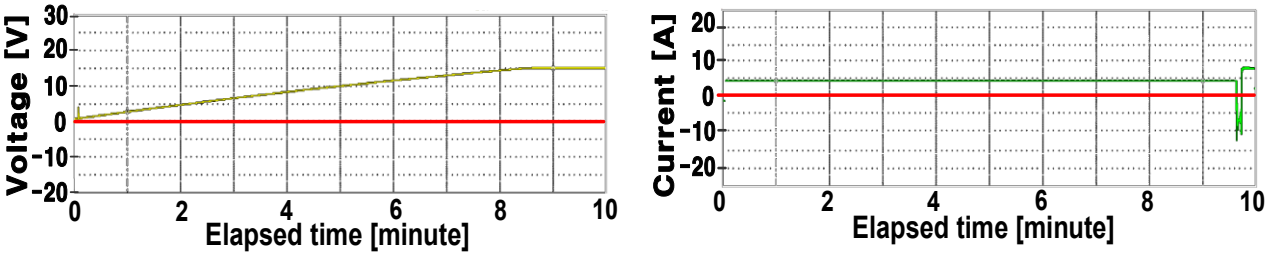

Fig. 6 Experimental voltage and current profiles during the charging process of a single supercapacitor..

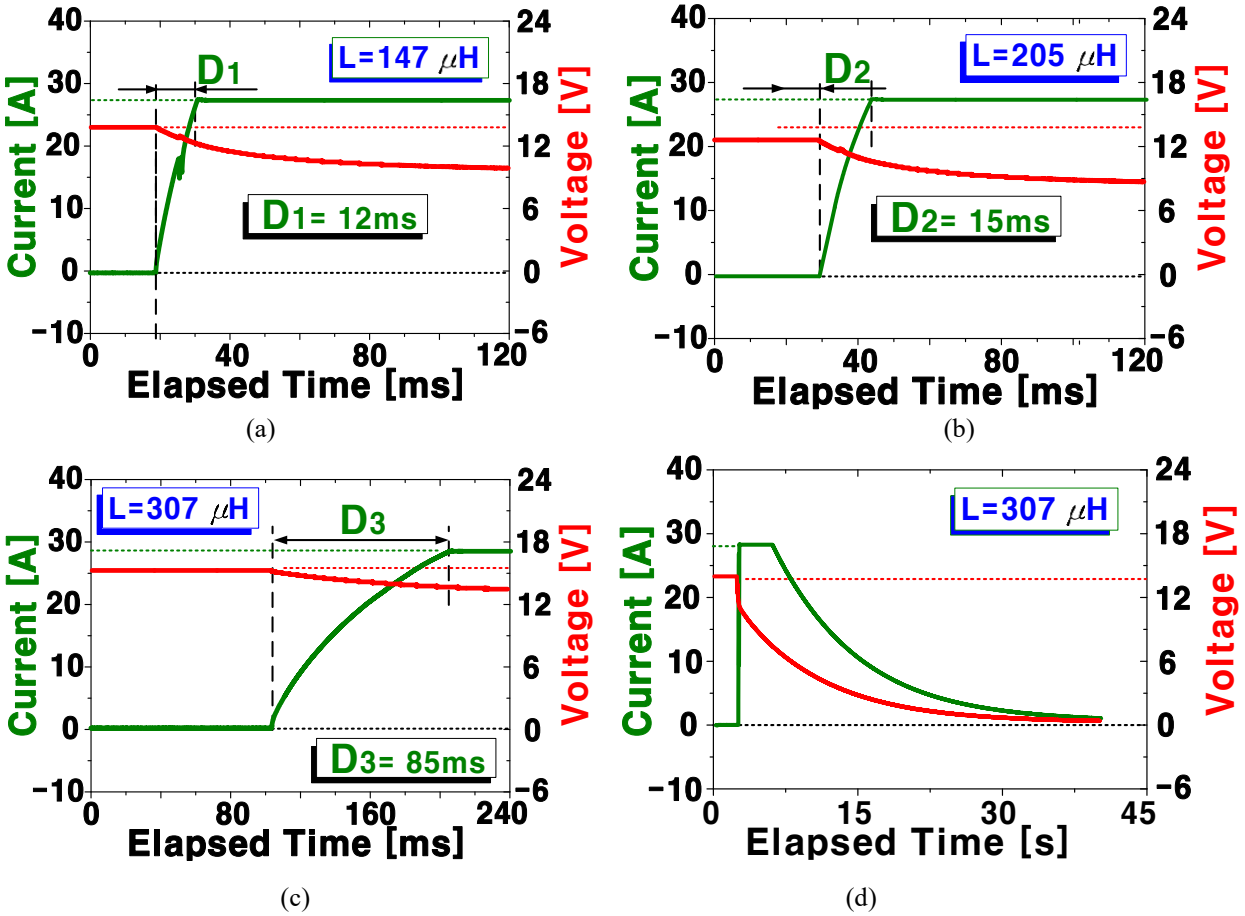

Fig. 7 Experimental results of voltage and current distributions during the supercapacitor discharging process under varying load inductances: inductance values of (a) load A = 147 μH, (b) load B = 205 μH, (c) total inductance of two inductors connected in series L = 307 μH, (d) complete discharging behavior at L = 205 μH over the full time duration.

The peak currents achieved under these conditions were 28.5 A, 28.0 A, and 28.3 A. These findings clearly demonstrate that as the inductance of the load magnet increases, the charging rate of the ramping current decreases even within a relatively short duration. Additionally, Fig. 7(d) shows that during the energy transfer process, the output voltage from the supercapacitor decreases rapidly and consistently, confirming the device's high discharge rate. However, this high-speed energy transfer, when directly applied to a superconducting magnet, may induce quenching due to abrupt thermal or electromagnetic disturbances. Therefore, the experimental results underscore the critical need for a discharge control system to moderate the energy transfer rate and ensure the safe and stable operation of the superconducting magnet system.

4. Conclusions

In this study, the feasibility and temporal characteristics of energy accumulation in the FC-PCS were experimentally investigated using a 370 kHz, 200 W RF generator in combination with a single 58 F supercapacitor unit. The system's performance was evaluated under varying inductive load conditions to assess the charging behavior and energy delivery profiles. During the wireless charging of the supercapacitor, it was found to be critical to maintain the output voltage within the rated tolerance in order to avoid thermal buildup and ensure stable operation. The results confirm that even a relatively low-capacity RF power source can effectively charge one or more supercapacitors when coupled with an appropriate rectification circuit and a voltage regulation controller, including a voltage divider module.

Furthermore, the duration required to fully charge the supercapacitor was found to be dependent primarily on the magnitude of the charging current, provided that the voltage remains below the rated threshold. This implies that current regulation is a key parameter in optimizing the charging time without compromising the safety or longevity of the energy storage unit. Also, since the current charging duration of supercapacitor is below 200 ms, high speed superconducting persistent current switch (PCS) should be required to keep charging current in the superconducting magnet.

Based on the experimental observations, it is anticipated that the incorporation of additional control components such as power relays and resistive attenuators integrated with current-voltage regulation circuits will be necessary to ensure safe and consistent charging of the HTS magnets. These components would be particularly useful in applications requiring high energy density or in scenarios where persistent current decay must be compensated during magnet operation. Given the inherently low resistance of HTS magnets, the delivery of high current potentially up to 200 A from the supercapacitor poses a significant risk of inducing a quench event. As well as, the design of the superconducting PCS and current divider module is required to save the high current in the superconducting magnet under short charging durations. Therefore, mitigating this risk through controlled power delivery is imperative. As a future direction, the authors intend to investigate the charging performance of multiple supercapacitors connected in series for a full-scale HTS levitation magnet system including superconducting PCS and current divider module, aiming to achieve stable energy transfer via wireless power technology without triggering a quench.

References

Suyong Choi, Minki Cho and Jungyoul Lim, Electromagnetic drag forces between HTS magnet and tube infrastructure for hyperloop, Scientifc Reports, Nature Portfolio, Vol.13 (2023), Article No.12626.

Ingo A. Hansen, Hyperloop transport technology assessment and system analysis, Journal of Transportation Planning & Technology, Vol.43, No.8 (2020), pp.803-820.

Konstantinos Gkoumas, Hyperloop academic research: A systematic review and a taxonomy of issues, Applied. Science. Vol.11, Issue (13), (2021), Article No.11135951.

A. Tsukamoto, S. Adachi, Y. Oshikubo, T. Hato, K. Tanabe, and K. Enpuku, High-temperature superconducting gradiometer coupled with large pickup coil made of GDBCO coated conductor, IEEE Transactions on Applied Superconductivity, Vol.21, No.3 (2011), pp. 358–362.

M. Igarashi et al., Persistent current HTS magnet cooled by cryocoler (1)- project overview, IEEE Transactions on Applied Superconductivity, Vol.15, No.2 (2005), pp. 1469– 1472.

T. Gong et al., Electromagnetic investigation of a high-temperature superconducting linear synchronous motor for high-speed railway, IEEE Transactions on Applied Superconductivity, Vol.28, No.3 (2018), Article No. 5202305.

C. Y. Lee, J. H. Lee, J. M. Jo, C. B. Park, W. H. Ryu, Y. D. Chung, Y. J. Hwang, T. K. Ko, S. Y. Oh, and J. Lee, Conceptual design of superconducting linear synchronous motor for 600-km/h wheel-type railway, IEEE Transactions on Applied Superconductivity, Vol.24, No.3 (2014), Article No. 3600304.

T. Gong et al., Electromagnetic investigation of a high-temperature superconducting linear synchronous motor for high-speed railway, IEEE Transactions on Applied Superconductivity, Vol.28, No.3 (2018), Article No. 5202305.

B. Shen et al., A novel all-superconducting propulsion and protection system for the HTS Maglev; concept, experimental verification and planning, IEEE Transactions on Applied Superconductivity, Vol.31, No.8 (2021), Article No. 3603405.

Y. D. Chung, C. Y. Lee, H. K. Kang, Y. G. Park, Design considerations of superconducting wireless power transfer for electric vehicle at different inserted resonators, IEEE Transactions on Applied Superconductivity, Vol.26 (2016), Article No. 0603605.

T. Strasser, F. Andren, J. Kathan, C. Cecati, C. Buccella, P. Siano, ´ P. Leitao, G. Zhabelova, V. Vyatkin, P. Vrba et al., A review of architectures and concepts for intelligence in future electric energy systems, IEEE Transactions on

Industrial Electronics, Vol.62, No.4 (2014), pp. 2424–2438.
M. Ristic, Y. Gryska, J. V. McGinley, and V. Yufit, Supercapacitor energy storage for magnetic resonance imaging systems, IEEE Transactions on Industrial Electronics, Vol.61, No.8 (2014), pp. 4255–4264.
I. S. Ike, I. Sigalas, S. Iyuke, and K. I. Ozoemena, An overview of mathematical modeling of electrochemical supercapactors /ultracapacitors, Journal of Power Sources, Vol.273 (2015), pp. 264–277.
A. Hijazi, P. Kreczanik, E. Bideaux, P. Venet, G. Clerc, and M. Di Loreto, Thermal network model of supercapacitors stack, IEEE Transactions on Industrial Electronics, Vol.59, No.2 (2012), pp. 979–987.